

## Article

# A Spatial Bayesian Distributed Lag Non-Linear Model of Influenza Incidence in New South Wales, Australia, 2000–2023

Mohammad Afzal Khan <sup>1</sup>, Oyelola Adegbeye <sup>2</sup>, Shiyang Lyu <sup>1</sup>, Kiki Maulana Adhinugraha <sup>3</sup>, David Taniar <sup>1</sup> and Theophilus I. Emeto <sup>4,5,\*</sup>

<sup>1</sup> Faculty of Information Technology, Monash University, Melbourne, VIC 3800, Australia; mkha0168@student.monash.edu (M.A.K.); arthur.lyu@monash.edu (S.L.); david.taniar@monash.edu (D.T.)

<sup>2</sup> Menzies School of Health Research, Charles Darwin University, Darwin, NT 0800, Australia; oyelola.adegbeye@menzies.edu.au (O.A.)

<sup>3</sup> School of Computing and Information Technology, La Trobe University, Melbourne, VIC 3086, Australia; K.Adhinugraha@latrobe.edu.au (K.M.A.)

<sup>4</sup> Australian Institute of Tropical Health and Medicine, James Cook University, Townsville, QLD 4811, Australia

<sup>5</sup> WHO Collaborating Centre for Vector-Borne and Neglected Tropical Diseases, James Cook University, Townsville, QLD 4811, Australia

\* \* Correspondence: theophilus.emeto@jcu.edu.au

**Abstract: Background and Objectives:** Influenza activity in temperate Australia varies markedly from year to year, yet the short-lag contribution of local weather remains uncertain; we therefore quantified the delayed and non-linear effects of temperature, relative humidity and rainfall on monthly notifications across the 15 Local Health Districts (LHDs) of New South Wales (NSW) during 2000–2023. **Materials and Methods:** Over 1.2 million laboratory-confirmed cases from the NSW Notifiable Conditions Information Management System were linked to district-level meteorological records and analysed with a spatial Bayesian distributed-lag non-linear model that used cross-basis splines (lags 04 weeks) and conditional autoregressive priors so neighbouring LHDs could borrow strength; four designs (case-crossover vs. time-series, with or without spatial pooling) were compared by deviance-information criterion. **Results:** The spatial case-crossover specification provided the best fit (DIC 153); temperature was the dominant driver, with cumulative relative risk (RR) peaking at 1.9 (95 % credible interval 1.42–2.5) near 21 °C and falling below 1.0 for <10 °C or >28 °C; humidity showed modest, location-specific effects (RR 1.31–1.6 between 55 % and 75 %), while rainfall was only sporadically associated with risk; spatial pooling removed implausible extremes in data-sparse western districts and produced coherent coastal hot-spots. **Conclusions:** Short-term weather fluctuations especially moderate ambient temperatures substantially modulate influenza transmission in NSW, and modelling frameworks that integrate lag structure, non-linearity and spatial dependence can underpin early-warning dashboards capable of anticipating district-level surges weeks in advance.

Received:

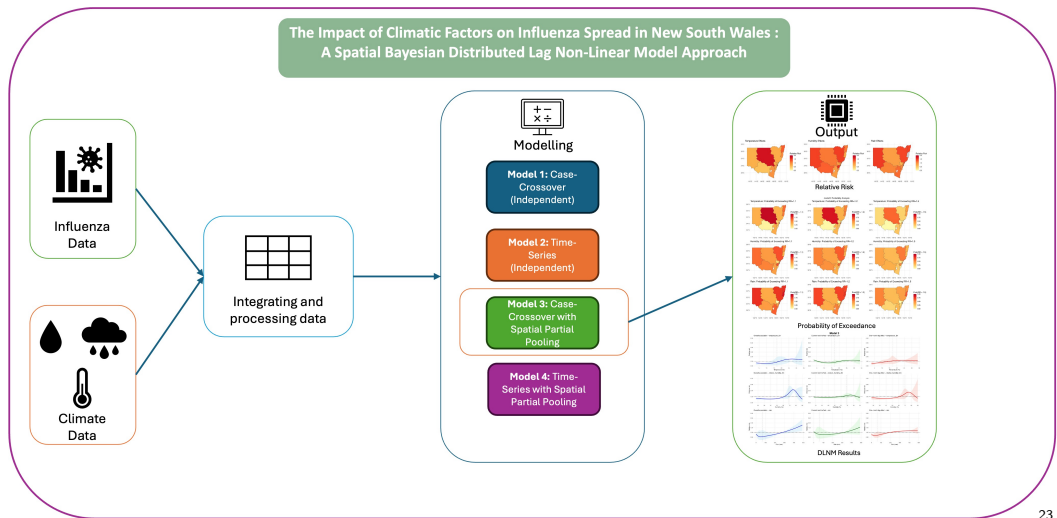
Accepted:

Published:

**Citation:** Khan, M.A.; Adegbeye, O.; Lyu, S.; Adhinugraha, K.M.; Taniar, D.; Emeto, T.I. Khan *et al.* Spatial Bayesian DLNM of Influenza in NSW (2000–2023). *Medicina* *xx*.

**Copyright:** © 2025 by the authors. Submitted to *Medicina* for possible open access publication under the terms and conditions of the Creative Commons Attribution (CC BY) license (<https://creativecommons.org/licenses/by/4.0/>).

**Keywords:** influenza epidemiology; climatic drivers; spatial Bayesian model distributed lag nonlinear model; New South Wales; Bayesian modelling; climate drivers; distributed-lag;



## 1. Introduction

Influenza remains a major public health burden worldwide, particularly in temperate regions, where seasonal outbreaks strain healthcare systems, escalate hospitalisations, inflate economic costs, and contribute to increased mortality [1,2]. A comprehensive understanding of the environmental drivers of influenza transmission is crucial for developing effective surveillance systems, early warning mechanisms, and targeted intervention strategies. In numerous temperate climates, influenza virus proliferation is favoured by specific meteorological conditions, notably lower temperatures and reduced humidity [3,4]. However, the precise nature of these interactions is complex and often characterised by non-linear dynamics [3,4].

Conversely, in subtropical and tropical settings, transmission may be governed by higher humidity and temperature thresholds [5], highlighting the geographical variability in climate-disease relationships. Moreover, rainfall patterns can influence influenza spread, albeit through more subtle or region-specific pathways [6]. Collectively, temperature, humidity, and precipitation have the potential to modulate both the magnitude and temporal dynamics (including lag effects) of influenza transmission, rendering simplistic linear or static models inadequate. [7] Australia has experienced significant fluctuations in influenza incidence in recent years. The 2019 season witnessed a severe outbreak, with approximately 313,000 laboratory-confirmed cases, followed by historically low incidence rates during 2020 and 2021, attributable to COVID-19 mitigation measures [8,9]. Subsequent seasons in 2022 and 2023 exhibited irregular patterns, including delayed peaks and prolonged transmission periods [10], while 2024 recorded approximately 148,700 cases with a test positivity rate of approximately 9.7%. These variations underscore the inherent unpredictability of influenza transmission and highlight the need for robust surveillance and analytic methodologies to inform public health responses [1].

Short-lag climate fluctuations play a crucial role in influenza surges [11,12]; however, modelling these effects presents several methodological challenges. The relationship between climatic factors and influenza is often non-linear, exhibiting threshold effects that may be overlooked by conventional regression techniques [13]. Additionally, climate-derived lag effects can extend over several days or weeks, complicating causal attribution. Substantial regional heterogeneity further compounds modelling complexities, as some local health districts manifest more pronounced seasonal variations or are characterised by sparse data, limiting precise parameter estimation [14]. While traditional case-crossover

and time-series approaches can mitigate temporal confounding within regions, they often neglect spatial dependencies. Conversely, purely spatial models may fail to account for short-lag temporal effects.

Recent advances in Spatial Bayesian Distributed Lag Non-Linear Models (SB-DLNMs) [15], an extension of Distributed Lag Non-Linear Model (DLNM) proposed by [13], offer a unified framework for integrating non-linear exposure-response functions, lag structures, and spatial pooling. These models account for spatial heterogeneity by enabling neighboring regions to "borrow strength" through hierarchical or conditional autoregressive priors, facilitating a more refined assessment of the influences of climatic variability on influenza risk [13,15]. Many previous studies have relied on traditional time-series or case-crossover designs, which lack spatial considerations and fail to capture the localised and non-linear nature of influenza-climate interactions [16–18]. This study aims to address this gap by employing a spatio-temporal modeling approach to quantify the impact of climate variability on influenza transmission across regions of New South Wales (NSW), Australia. By integrating non-linear splines, lag components, and spatial partial pooling, this framework provides a more comprehensive understanding of climatic drivers of influenza, thereby enhancing public health preparedness and intervention strategies.

## 2. Materials and Methods

### 2.1. Study area

This study examines New South Wales (NSW) ( $33.5^{\circ}\text{S}$ ,  $145.5^{\circ}\text{E}$ ), an Australian State focusing on its 15 local health districts. NSW is Australia's most populous state with 8.3 million residents and spans over  $801,150 \text{ km}^2$  along Australia's eastern seaboard characterized by a narrow coastal strip, the Great Dividing Range, agricultural plains, and semi-arid western regions. The state's residents are predominantly concentrated in urban centers, with housing in Greater Sydney ( $33.8^{\circ}\text{S}$ ,  $151.0^{\circ}\text{E}$ ) housing 66% of the population (5.3 million) within just  $12,400 \text{ km}^2$ . This urban-rural setting creates varying population densities in comparatively short stretches, from densely populated coastal cities. (400 people/ $\text{km}^2$  in Sydney) to sparse inland settlements (less than 1 person/ $\text{km}^2$ ). This state features diverse climatic zones that range from humid subtropical along the coast to cool temperate in highlands and arid conditions in western areas, making it an ideal setting for epidemiological modeling of climate-influenza relationships in different urban and peri-urban environments.

### 2.2. Data sources

#### 2.2.1. Influenza data

Data for this study were obtained from the NSW Health Notifiable Conditions Information Management System (NCIMS) [19]. Data were extracted separately for each of the 15 Local Health Districts (LHD) in NSW, with records spanning 2000 to 2023. The data sets included monthly influenza cases. Influenza incidence in NSW follows a strong seasonal pattern, with peaks during winter (June–August), including a surge in 2019 and record low cases in 2020–2021 due to COVID-19 mitigation strategies [1,8,9].

#### 2.2.2. Climate data

Monthly climate records were collected from the Australian Bureau of Meteorological, covering the same 15 LHDs. Australia. Raw data consisted of 216,264 hourly observations from 17 weather stations, yielding approximately 3.67 million data points before processing. The dataset included temperature at 2 m (in degrees Celsius), relative humidity at 2 m (in percent), and rainfall or precipitation (in millimeters). To align with influenza case

reporting, the hourly temperature and humidity values were averaged to obtain monthly means, and rainfall was summed.

### 2.2.3. Data integration

Influenza and climate datasets were standardized, merged and prepared for analysis in Excel, structured to allow cross-basis expansion, lag computations and spatial alignment at LHDs level. The final integrated dataset (Figure 1) provides a robust framework for analysing the relationship between meteorological variables and influenza incidence in NSW.

### 2.2.4. Spatial Adjacency

To incorporate spatial dependencies, we constructed an adjacency matrix using NSW LHD boundary shapefiles, defining neighbouring districts  $N(i)$  for each LHD. This spatial framework facilitated the use of hierarchical and conditional autoregressive (CAR) priors, which smooth estimates across geographically contiguous regions, enhancing stability in data-sparse areas [14].

## 2.3. Modeling Framework

Our modelling framework employs a Spatial Bayesian Distributed Lag Non-Linear Model (SB-DLNM)[15] to capture both the delayed and non-linear effects of climatic variables on influence incidence in NSW while accounting for spatial dependencies across several health districts. Given  $y_{i,t}$ , the number of influenza cases in LHD  $i$  at time  $t$ , we assume a Poisson likelihood

$$y_{i,t} \sim \text{Poisson}(\lambda_{i,t}), \quad \log(\lambda_{i,t}) = \eta_{i,t}.$$

The linear predictor  $\eta_{i,t}$  incorporates non-linear, lagged climate effects through cross-basis expansions. For each climate variable  $X_{v,i,t}$  (with  $v \in \{\text{temperature, humidity, rainfall}\}$ ), we define a cross-basis function

$$\mathbf{cb}_{v,i,t} = \text{crossbasis}(X_{v,i,t}; L),$$

where  $L$  is the maximum lag (e.g., one month) and the expansion captures both the non-linear exposure-response relationship and the delayed effect of the climate variable.

Similar to [15], in this study, we use two different designs, case-crossover and time-series designs.

For the case-crossover models, each record is assigned to a stratum defined by the LHD, month, and year, with a stratum-specific intercept  $\alpha_{\text{stratum}(i,t)}$  absorbing local time-invariant factors. The linear predictor in this setting is as follows:

$$\zeta_{i,t} = \alpha_{\text{stratum}(i,t)} + \mathbf{b}_{\text{temp},i}^\top \mathbf{cb}_{\text{temp},i,t} + \mathbf{b}_{\text{hum},i}^\top \mathbf{cb}_{\text{hum},i,t} + \mathbf{b}_{\text{rain},i}^\top \mathbf{cb}_{\text{rain},i,t}.$$

For the time-series models, monthly intercepts  $\alpha_{i,m(t)}$ , trend splines, and seasonal basis functions are incorporated to capture longer-term effects. The model is specify as follows:

$$\gamma_{i,t} = \alpha_{i,m(t)} + \mathbf{b}_{\text{temp},i}^\top \mathbf{cb}_{\text{temp},i,t} + \mathbf{b}_{\text{hum},i}^\top \mathbf{cb}_{\text{hum},i,t} + \mathbf{b}_{\text{rain},i}^\top \mathbf{cb}_{\text{rain},i,t} + \Gamma_i^\top \mathbf{t}_t + \Delta_{i,y(t)}^\top \mathbf{s}_{m(t)}.$$

In Models 3 and 4, spatial partial pooling is implemented by assigning hierarchical priors to coefficient vectors  $\{\mathbf{b}_{\text{temp},i}, \mathbf{b}_{\text{hum},i}, \mathbf{b}_{\text{rain},i}\}$  of the form

$$\mathbf{b}_{v,i} = \boldsymbol{\mu}_v + \sigma_v \boldsymbol{\theta}_{v,i}, \quad \boldsymbol{\theta}_{v,i} \sim \mathcal{N}(\mathbf{0}, \tau_v^{-1} \mathbf{I}),$$

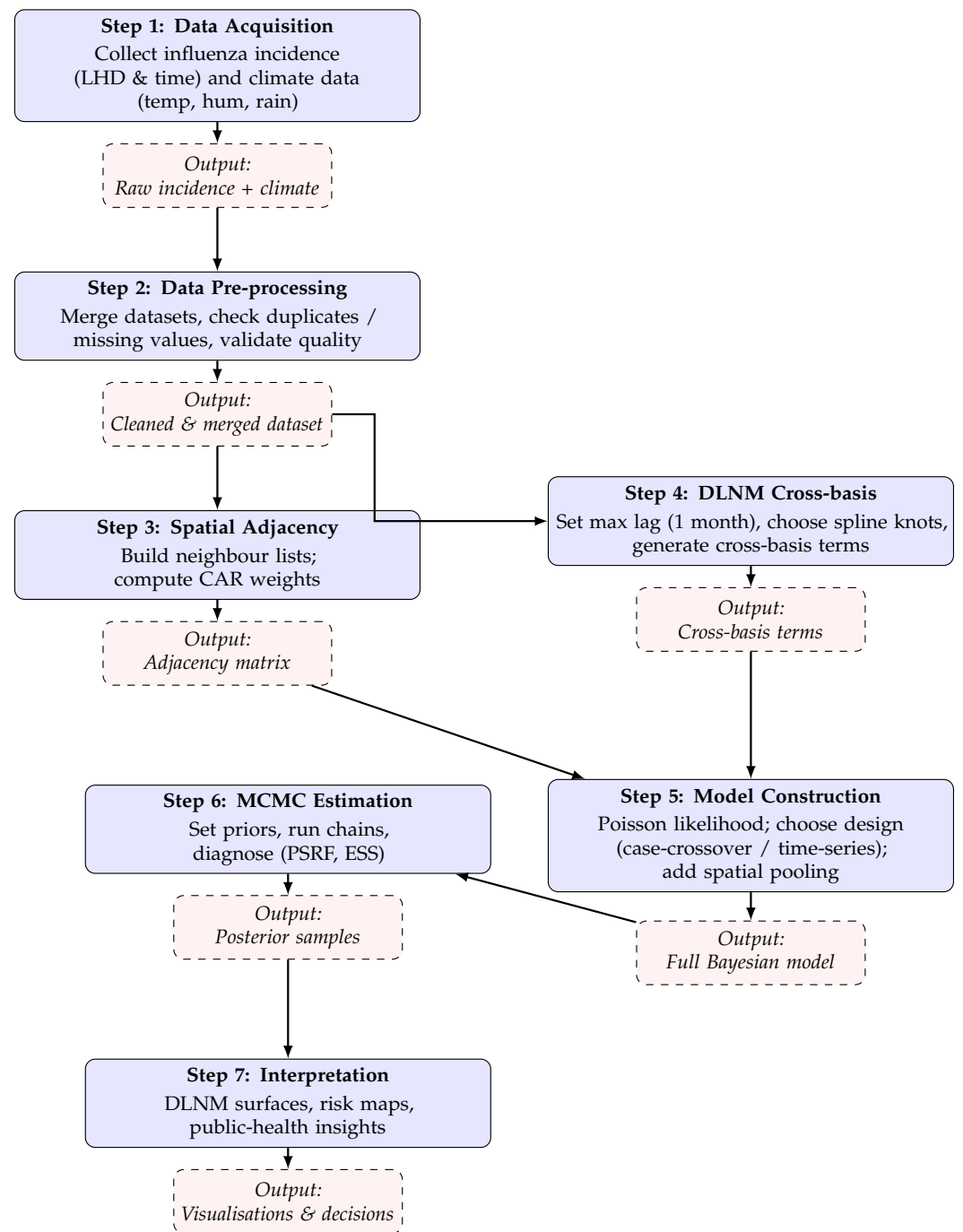


**Figure 1.** Detailed methodology flowchart for the spatial Bayesian DLNM.

or through a CAR structure. This approach stabilizes estimates in data-sparse areas, while still allowing for genuine local heterogeneity.

#### 2.4. Model specification

We fitted four models to examine how short-term climate fluctuations in temperature, humidity, and rainfall affect influenza incidence across LHDs in NSW. Two models (Models 1 and 3) adopt a case-crossover design to detect short-lag, within-LHD climatic effects. At the same time, Models 2 and 4 rely on a time-series design to capture longer-term or seasonal climate trends. Model 1 employs an independent case-crossover approach that estimates acute climate-disease relationships within each LHD separately, without borrowing information from neighbouring districts [20]. In contrast, Model 2 uses an independent time-series framework that focuses on extended lags and seasonal influences within each LHD [21]. Model 3 builds on the case-crossover design by incorporating spatial partial pooling through hierarchical (CAR) priors to share information among neighbouring LHDs, thereby stabilizing estimates in data-sparse regions [14]. Finally, Model 4 combines a time-series design with spatial partial pooling to moderate outlier estimates in smaller LHDs while reflecting broader climate patterns in areas with limited data. By comparing these four models, we assess the performance of short-lag versus longer-term approaches (case-crossover versus time-series) under independent and spatially pooled structures. This comprehensive framework provides valuable insights into how temperature, humidity, and rainfall drive influenza incidence across diverse LHDs in NSW, even in regions where data remain limited, and is supported by recent work showing that climate variability can significantly alter viral transmission dynamics [3,4].

#### 2.5. Model priors and strategies

All models are estimated under a Bayesian paradigm using Markov chain Monte Carlo (MCMC) methods. Prior distributions are typically set as  $\text{Normal}(0,0.001)$  for intercepts and climate coefficients, with variance hyperparameters assigned  $\text{Gamma}(0.1,0.1)$  or  $\text{Uniform}(0,10)$  priors. Multiple MCMC chains are run in parallel, with convergence assessed using the Gelman-Rubin statistic and effective sample size diagnostics. Posterior inference focuses on key outputs such as relative risk (RR) estimates, where, for example, the RR for temperature in a given LHD is calculated as

$$\text{RR}_{\text{temp},i}(x) = \exp \left[ \mathbf{b}_{\text{temp},i}^\top (\mathbf{c}\mathbf{b}_{\text{temp}}(x) - \mathbf{c}\mathbf{b}_{\text{temp}}(x_0)) \right],$$

and the probability that these RR values exceed clinically significant thresholds (e.g.,  $\text{RR} > 1$ , 95th percentile). Risk maps and other visual outputs are generated to aid interpretation, and all analyses ensure that temporal alignment and spatial adjacency are rigorously maintained.

### 3. Results

#### 3.1. Model Convergence and Goodness of Fit

All models were estimated under a Bayesian framework using MCMC methods with multiple chains to ensure robust posterior exploration. Table 1 summarises both convergence diagnostics and deviance-based goodness-of-fit measures for the four models. The convergence metrics reported include the Potential Scale Reduction Factor (PSRF), Effective Sample Size (ESS), Monte Carlo Error (MC Error), median posterior standard deviation (Med SD), median credible interval width (Med CI Width), and median lag-1 autocorrelation (Med Autocorr). In parallel, model fit was evaluated using the Deviance Information Criterion (DIC), Bayesian Information Criterion (BIC), and Quasi-Akaike Information Crite-

rion (QAIC). Notably, Models 1 and 3, which employ case-crossover designs, demonstrated faster convergence and improved fit relative to the longer-horizon time-series models (Models 2 and 4), with Model 3's spatial partial pooling further stabilizing estimates in data-sparse regions. These results are consistent with previous work suggesting that short-lag, within-LHD signals are more readily detectable and benefit from spatial smoothing [11,14,22,23].

**Table 1.** Diagnostics and deviance-based criteria for model evaluation

Model	Convergence			Posterior			Model Fit		
	PSRF	ESS	MCE	SD	CI	Auto	DIC	BIC	QAIC
Model 1 (CCO)	20.49	4.52	0.017	1.44	4.79	0.980	23 808	20 542	27 480
Model 2 (TS)	50.72	4.78	0.014	1.17	4.01	0.994	81 603	64 642	99 560
Model 3 (SCCO)	24.05	4.47	0.012	1.04	3.58	0.958	23 655	20 621	27 178
Model 4 (STS)	23.92	4.37	0.009	0.76	2.77	0.987	82 773	64 985	101 639

### 3.2. Single-Variable Exposure-Response Curves across All Models

Figure 2 display the exposure-response relationships between influenza risk and climatic variables (temperature, humidity, and rainfall) as estimated by the four models. In Model 1, which adopts an independent case-crossover design focusing on short-lag exposures, the temperature response curve shows a gradual increase in RR around midrange temperatures (1520°C). However, the confidence intervals widen at the extremes (e.g., near 35°C). The humidity relationship remains relatively flat at moderate levels but slightly increases near higher exposures (8090%). Similarly, the rainfall association follows a mild J-shaped trend, with a dip around 50 mm followed by an increase near 200300 mm, possibly reflecting short-term changes in indoor crowding after precipitation events [4].

Considering Model 2 employs an independent time-series approach to capture longer-term climatic influences, the overall temperature effect peaks around 1520°C, consistent with findings that cool-to-mild conditions may enhance influenza transmission [3]. The comparison of current-month and one-month lag effects suggests that influenza risk is more strongly associated with sustained temperature regimes than rapid, short-term fluctuations. For humidity, the model reveals a steep increase in RR at exposures exceeding 8090%, with some estimates reaching very high values. The rainfall curve in Model 2 peaks in the moderate range (50150 mm) before declining at very high precipitation levels ( $\geq 300400$  mm), indicating that while moderate seasonal rainfall could promote transmission, very heavy rainfall might limit outdoor interactions and thereby reduce risk [6].

Model 3 combines a case-crossover design with spatial partial pooling to stabilize estimates across regions with varying data densities. In this model, the temperature-response curve increases steadily from around 10°C to 30°C, with the overall RR reaching about two at higher temperatures. Although the current-month effects remain relatively flat across much of the temperature range, the one-month lag effect shows a moderate increase around 2025°C, suggesting that influenza risk may be more sensitive to temperature changes occurring one to two weeks prior [3]. The humidity effect in Model 3 displays an upward trend between 60% and 80%, in line with laboratory evidence on influenza viability [4]. The rainfall association in this model follows a modest J-shaped pattern, with a peak relative risk of approximately 1.52.0 occurring near 300400 mm. Thus, the combination of short-lag sensitivity and spatial smoothing in Model 3 effectively captures immediate weather triggers while mitigating volatile estimates in low-data regions.

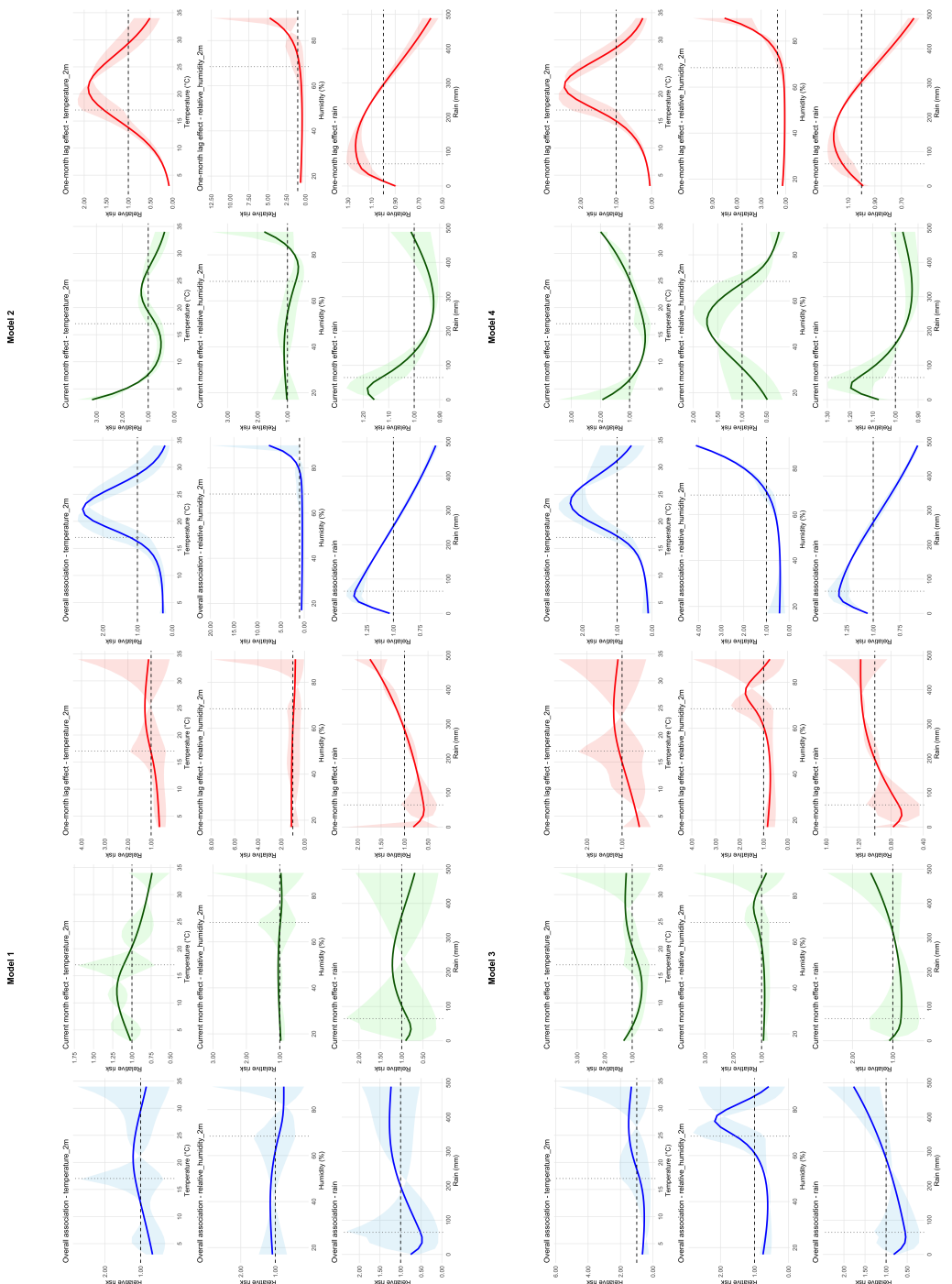


**Figure 2.** Cummulative RR for Model 1,2,3 and 4. The figure illustrates the complex interactions between climatic variables and risk over time. Model 4 exhibits a strong effect of relative humidity and temperature compared to other models.

Finally, Model 4 applies a time-series approach with spatial partial pooling to examine seasonal climate effects. The temperature response in Model 4 also peaks around  $1520^{\circ}\text{C}$ , with spatial pooling smoothing out unrealistic values at temperatures above  $30^{\circ}\text{C}$ . For humidity, the model continues to show a strong increase in relative risk at exposures above 80%, though these estimates are moderated compared to those in the independent time-series model. The rainfall association in Model 4 mirrors that of Model 2, with a moderate peak at 50150 mm followed by a decline at very high rainfall levels ( $\geq 300$  mm), resulting in a more coherent regional pattern.

222  
223  
224  
225  
226  
227  
228

### 3.3. Spatial Case-Crossover Insights

Given the above comparative assessments, we place greater emphasis on Model 3s (hereafter referred to as the SCCO model). In what follows, we illustrate how temperature, humidity, and rainfall, when modelled under a short-lag, spatial partial pooling design, shape district-level influenza risks. Figure 3 displays the district-level risk maps produced under Model 3 for the three climate variables. The spatial partial pooling removes the abrupt checkerboard patterns observed in earlier models when data-scarce LHDs encountered extreme climate conditions. This smoothing effect is particularly evident in regions such as Far West and Murrumbidgee, where limited observations might otherwise lead to inflated or deflated RR estimates [22]. Spatial maps of relative risk (RR) are expanded upon in the Supplementary Material (Section A, Fig. 1–3), where we show how partial pooling smooths out outlier estimates in data-scarce LHDs.

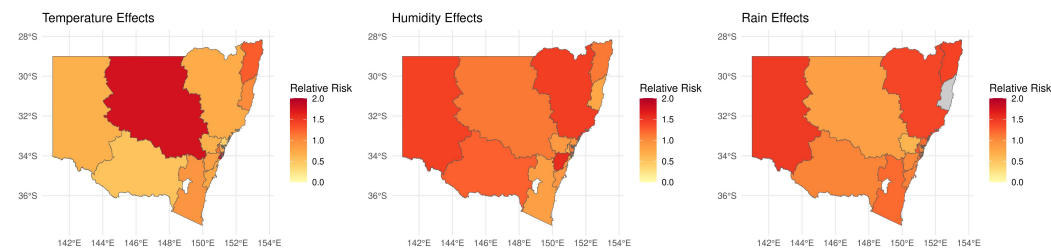


**Figure 3.** District-level risk maps under Model 3 (partial pooling). Darker regions indicate higher relative risk (RR).

**Table 2.** Probability of Exceeding Selected RR Thresholds under Model 3. Values reflect the posterior probability (in %) that the short-lag RR exceeds 1 for each climate variable.

LHD	Variable	Threshold	Exceed Prob (%)	Comments
Central Coast	Humidity	1.0	100.0	Very high
	Rain	1.0	55.7	Moderate
	Temperature	1.0	94.0	Very high
Far West	Humidity	1.0	91.7	Very high
	Rain	1.0	93.8	Very high
	Temperature	1.0	66.7	Moderate
Hunter NE	Humidity	1.0	40.2	Moderate
	Rain	1.0	35.3	Low
	Temperature	1.0	66.7	Moderate
Illawarra S.	Humidity	1.0	33.3	Low
	Rain	1.0	52.3	Moderate
	Temperature	1.0	79.0	High
Mid North Coast	Humidity	1.0	48.4	Moderate
	Rain	1.0	100.0	Very high
	Temperature	1.0	84.8	High
Murrumbidgee	Humidity	1.0	53.1	Moderate
	Rain	1.0	63.4	Moderate
	Temperature	1.0	52.5	Moderate
Nepean Blue Mts	Humidity	1.0	76.1	High
	Rain	1.0	51.6	Moderate
	Temperature	1.0	100.0	Very high
Northern NSW	Humidity	1.0	33.3	Low
	Rain	1.0	100.0	Very high

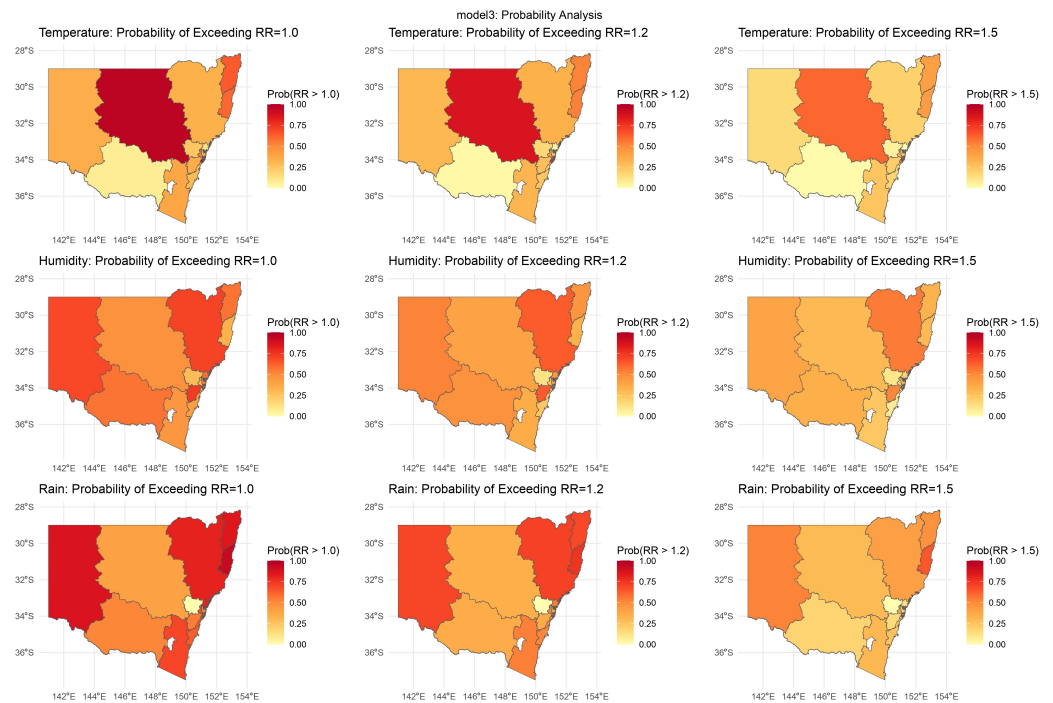
Continued on next page

Table 2 – continued from previous page

LHD	Variable	Threshold	Exceed Prob (%)	Comments
Northern Sydney	Temperature	1.0	96.3	Very high
	Humidity	1.0	66.7	Moderate
	Rain	1.0	36.5	Low
	Temperature	1.0	81.1	High
SE Sydney	Humidity	1.0	9.0	Very low
	Rain	1.0	66.7	Moderate
	Temperature	1.0	79.0	High
SW Sydney	Humidity	1.0	78.9	High
	Rain	1.0	58.9	Moderate
	Temperature	1.0	94.4	Very high
Southern NSW	Humidity	1.0	40.1	Moderate
	Rain	1.0	96.3	Very high
	Temperature	1.0	40.8	Moderate
Sydney	Humidity	1.0	14.0	Low
	Rain	1.0	99.2	Very high
	Temperature	1.0	99.9	Very high
Western NSW	Humidity	1.0	54.7	Moderate
	Rain	1.0	26.1	Low
	Temperature	1.0	53.6	Moderate
Western Sydney	Humidity	1.0	49.9	Moderate
	Rain	1.0	55.3	Moderate
	Temperature	1.0	39.3	Low

The posterior probability that the RR exceeds thresholds of 1.0, 1.2, or 1.5 in each LHD is presented in Table 2 under Model 3. For instance, in coastal districts such as Central Coast and Illawarra Shoalhaven the probability that RR exceeds 1.0 is very high when temperature is around 15–20°C or when humidity is in the midrange (50–80%), which aligns with experimental findings on influenza viability [3,4]. In contrast, certain inland or highrainfall districts exhibit lower exceedance probabilities, reflecting less consistent climate triggers and the moderating impact of spatial partial pooling.

Figure 4 further illustrates the spatial distribution of the probability that the relative risk exceeds different thresholds (1.0, 1.2, and 1.5) for temperature, humidity, and rainfall. The colour gradient, ranging from yellow (low probability) to red (high probability), reveals that high probabilities are predominantly found in northern and coastal regions. This spatial variation underscores the heterogeneous impact of extreme climate conditions on influenza risk and offers valuable insights for targeted public health interventions.



**Figure 4.** Spatial distribution of the probability of RR exceeding thresholds (1.0, 1.2, and 1.5) for temperature, humidity, and rainfall under Model 3. Each row represents a different climate variable, while each column corresponds to a specific RR threshold. The maps indicate the probability that the relative risk surpasses the given threshold, with a colour gradient ranging from yellow (low probability) to red (high probability). High probabilities are observed in specific regions, particularly in northern and coastal areas, suggesting spatial variations in climate risk. These findings highlight the potential health or environmental impacts of extreme climate conditions across different regions.

Additional insights into the moderating effect of spatial partial pooling are provided by examining the short-lag relative risks at the 1st percentile ( $p_1$ ) and 5th percentile ( $p_5$ ) of climate exposures. Table ?? presents these estimates for temperature, humidity, and rainfall across various LHDs. For example, in Far West, the independent model previously produced an extreme RR of over 472,000 for moderate rainfall (64.08 mm). Still, spatial partial pooling reduces this to a more plausible estimate of approximately 27. Similarly, on the Central Coast, humidity at the  $p_1$  level (57.18%) yields an RR of roughly 1.12, which, while still elevated, is moderated by hierarchical shrinkage. These examples demonstrate that although local signals persist, such as the risk elevation associated with high humidity, the incorporation of spatial partial pooling ensures that estimates remain both biologically plausible and methodologically stable [22].

255  
256  
257  
258  
259  
260  
261  
262  
263  
264  
265

**Table 3.** P<sub>1</sub> and P<sub>5</sub> estimates from Model 3

LHD	Variable	P <sub>1</sub> value	P <sub>1</sub> RR (95% CI)	P <sub>5</sub> value	P <sub>5</sub> RR (95% CI)	Comments
Central Coast	Temperature	11.71 °C	2.55 (0.53, 6.47)	12.38 °C	10.34 (0.69, 34.20)	Mild cold; risk increases with warming
Central Coast	Humidity	57.18 %	1.12 (0.88, 1.28)	61.92 %	0.92 (0.78, 1.15)	Normal humidity; minimal effect
Central Coast	Rainfall	5.24 mm	0.69 (0.24, 1.52)	12.62 mm	0.62 (0.15, 1.84)	Low rainfall; minimal risk
Far West	Temperature	9.98 °C	2.04 (0.11, 7.79)	10.69 °C	2.72 (0.09, 10.67)	Cold; slight risk; high uncertainty
Far West	Humidity	23.16 %	2.87 (0.16, 9.33)	27.61 %	3.14 (0.08, 14.59)	Very dry; elevated risk; wide CI
Far West	Rainfall	0.00 mm	2.07 (0.00, 27.99)	0.40 mm	19.79 (0.00, 27.43)	Extreme drought; high risk
Hunter New England	Temperature	8.12 °C	3.10 (0.58, 9.18)	9.02 °C	11.19 (1.27, 35.12)	Cold; risk rises with warming
Hunter New England	Humidity	40.34 %	0.98 (0.47, 2.28)	47.56 %	2.80 (0.46, 8.19)	Dry; moderate risk at P <sub>5</sub>
Hunter New England	Rainfall	1.02 mm	2.08 (0.02, 15.65)	3.56 mm	1.84 (0.02, 13.57)	Very dry; moderate risk; wide CI
Illawarra	Temperature	10.16 °C	1.32 (0.55, 3.95)	11.12 °C	3.37 (1.22, 8.53)	Mild cold; risk increases with warming
Shoalhaven	Humidity	59.71 %	1.00 (0.98, 1.02)	62.47 %	1.00 (0.82, 1.28)	Normal humidity; minimal effect
Shoalhaven	Rainfall	5.18 mm	1.36 (0.21, 3.47)	12.78 mm	1.08 (0.14, 2.70)	Low rainfall; slight risk
Shoalhaven	Temperature	10.52 °C	3.58 (0.46, 11.22)	11.60 °C	12.71 (1.13, 49.77)	Mild cold; high risk at P <sub>5</sub>
Mid North Coast	Humidity	60.52 %	1.00 (0.91, 1.08)	65.46 %	1.09 (0.57, 1.75)	Normal humidity; minimal effect
Mid North Coast	Rainfall	1.78 mm	2.05 (0.49, 8.36)	6.02 mm	1.97 (0.46, 7.86)	Very dry; moderate risk; wide CI
Murramburidgee	Temperature	8.59 °C	1.94 (0.19, 7.40)	8.99 °C	2.74 (0.22, 9.63)	Cold; slight risk; high uncertainty
Murramburidgee	Humidity	31.97 %	1.74 (0.66, 3.13)	35.53 %	1.45 (0.40, 3.07)	Dry; slight risk
Murramburidgee	Rainfall	0.34 mm	8.73 (0.00, 103.55)	3.22 mm	9.16 (0.00, 109.46)	Extreme drought; very wide CI
Nepean Blue Mts	Temperature	6.73 °C	6.21 (1.32, 15.92)	7.68 °C	20.75 (2.12, 59.79)	Very cold; high risk
Nepean Blue Mts	Humidity	50.31 %	0.97 (0.46, 1.90)	59.53 %	1.00 (0.97, 1.03)	Moderately dry; minimal effect
Nepean Blue Mts	Rainfall	5.84 mm	1.86 (0.65, 4.31)	12.54 mm	2.24 (0.56, 6.55)	Low rainfall; moderate risk
Northern NSW	Temperature	12.29 °C	0.57 (0.24, 1.13)	13.08 °C	2.04 (0.31, 6.05)	Moderate temp; risk rises with warming
Northern NSW	Humidity	55.52 %	1.08 (0.95, 1.21)	60.62 %	0.98 (0.93, 1.04)	Normal humidity; minimal effect
Northern NSW	Rainfall	1.40 mm	0.73 (0.33, 1.46)	6.98 mm	0.69 (0.25, 1.47)	Very dry; potentially protective
Northern Sydney	Temperature	10.46 °C	4.09 (0.16, 13.59)	11.01 °C	9.72 (0.45, 35.88)	Mild cold; high risk; wide CI
Northern Sydney	Humidity	55.45 %	1.07 (0.92, 1.17)	61.06 %	0.96 (0.94, 1.00)	Normal humidity; minimal effect

*Continued on next page*

Table 3 – continued

LHD	Variable	P <sub>1</sub> value	P <sub>1</sub> RR (95 % CI)	P <sub>5</sub> value	P <sub>5</sub> RR (95 % CI)	Comments
Northern Sydney	Rainfall	2.90 mm	1.37 (0.14, 3.20)	8.50 mm	1.19 (0.08, 2.64)	Very dry; slight risk
SE Sydney	Temperature	12.15 °C	3.10 (0.20, 8.00)	13.04 °C	9.23 (0.32, 26.47)	Moderate temp; high risk at P <sub>5</sub>
SE Sydney	Humidity	57.84 %	0.87 (0.68, 1.11)	62.51 %	1.08 (0.91, 1.17)	Normal humidity; minimal effect
SE Sydney	Rainfall	3.88 mm	0.83 (0.41, 1.66)	8.02 mm	0.78 (0.33, 1.83)	Dry; minimal risk
SW Sydney	Temperature	14.30 °C	7.35 (2.97, 13.22)	14.91 °C	21.17 (4.81, 51.39)	Moderate temp; very high risk
SW Sydney	Humidity	61.95 %	1.15 (1.10, 1.21)	64.32 %	1.23 (1.11, 1.37)	Normal humidity; slight risk
SW Sydney	Rainfall	6.20 mm	1.40 (0.78, 2.19)	15.70 mm	1.33 (0.75, 2.05)	Low rainfall; slight risk
Southern NSW	Temperature	3.52 °C	7.61 (0.56, 23.14)	4.07 °C	9.95 (0.56, 31.01)	Extreme cold; very high risk
Southern NSW	Humidity	54.17 %	0.85 (0.32, 1.88)	61.41 %	1.03 (0.89, 1.13)	Moderately dry; minimal effect
Southern NSW	Rainfall	3.82 mm	1.65 (0.01, 10.19)	9.50 mm	1.67 (0.00, 8.46)	Dry; slight risk; wide CI
Sydney	Temperature	7.74 °C	3.53 (0.80, 9.44)	8.42 °C	7.34 (1.27, 21.95)	Very cold; high risk
Sydney	Humidity	55.34 %	0.84 (0.71, 0.98)	62.01 %	1.09 (0.94, 1.26)	Normal humidity; minimal effect
Sydney	Rainfall	3.64 mm	0.74 (0.37, 1.40)	8.04 mm	0.67 (0.27, 1.35)	Dry; potentially protective
Western NSW	Temperature	9.86 °C	1.18 (0.16, 4.26)	10.31 °C	1.57 (0.20, 5.81)	Cold; slight risk; high uncertainty
Western NSW	Humidity	27.00 %	2.32 (0.27, 6.48)	30.96 %	3.55 (0.29, 9.87)	Very dry; elevated risk
Western NSW	Rainfall	0.47 mm	10.17 (0.11, 49.89)	1.12 mm	9.16 (0.10, 45.82)	Extreme drought; very wide CI
Western Sydney	Temperature	11.00 °C	1.16 (0.29, 2.54)	11.59 °C	3.29 (1.21, 5.77)	Mild cold; risk increases with warming
Western Sydney	Humidity	56.49 %	1.15 (0.89, 1.40)	60.47 %	0.98 (0.95, 1.01)	Normal humidity; minimal effect
Western Sydney	Rainfall	3.87 mm	0.91 (0.21, 2.20)	9.44 mm	0.90 (0.17, 2.37)	Dry; minimal risk

Overall, these results demonstrate that spatial partial pooling in Model 3 protects against unrealistic or unbounded relative risk estimates, particularly in small-population LHDs. Although local signals such as the elevated risk associated with high humidity persist, using hierarchical priors ensures that estimates remain both biologically plausible and methodologically stable [22]. Comparisons of exposure extremes further illustrate how Model 3 moderates outliers while preserving meaningful local epidemiological trends.

### 3.4. Exposure–Lag–Response Curves and Maps

Figure 2 presents the final temperature and humidity lag surfaces for Model 3. These surfaces reveal that influenza risk peaks at temperatures between approximately 1022°C, with the effect diminishing at higher temperatures. Similarly, the risk is most sensitive to relative humidity levels in the range of 5080%. The contours across lags 03 weeks are reasonably smooth, which supports the operation of short-lag mechanisms in influenza transmission [11].

Detailed local health district-level risk analyses (Supplementary Material, Section D) illustrate how influenza risk evolves with climate exposure. illustrate how each local health districts posterior distribution evolves under short-lag climate changes. Although smaller districts exhibit broader intervals, spatial partial pooling prevents unrealistic or unbounded RR estimates under the hierarchical Bayesian principle of shrinkage [22]. These figures further indicate that, while inland and coastal regions may differ in their temperature influenza responses, the broad pattern of moderate temperature and moderate humidity is consistently associated with elevated short-lag risk. Maps comparing Model 1 vs. Model 3, as well as the single-variable cross-basis curves for each LHD, are provided in Supplementary section B–D.

## 4. Discussion

This study investigated the short-term influence of temperature, humidity, and rainfall on influenza incidence across NSW, Australia, employing a Spatial Bayesian Distributed Lag Non-Linear Model. Our methodology integrated (i) a case-crossover design to capture rapid climatic effects, (ii) cross-basis expansions for non-linear lagged responses, and (iii) spatial partial pooling across LHDs to address data sparsity. Findings indicate that mild-to-cool temperatures (1022°C) and moderate-to-high humidity levels (5080%) were consistently associated with elevated influenza risk, corroborating virological evidence on virus stability and droplet viability [3,4]. Spatial pooled models (particularly Model 3) provided the most stable estimates, mitigating extreme relative risk values in data-sparse regions. While rainfall exhibited some district-specific associations, its overall impact was weaker and more variable. These results highlight the importance of incorporating spatial smoothing in epidemiological models to enhance reliability and capture localised climate-influenza interactions [6].

### 4.1. Short-Lag Model Performance and Spatial Pooling Benefits

Comparisons across models demonstrated that short-lag case-crossover approaches (particularly Model 3) were more effective at detecting abrupt changes in influenza risk following shifts in temperature or humidity than longer-horizon time-series designs [11,12]. This align with experimental evidence regarding the virus sensitivity to brief climatic anomalies [3,24]. Notably, mild-to-cool temperature (10–22 °C) consistently correlated with increased influenza transmission within a few weeks, reinforcing established virological mechanisms.

A key strength of model 3s was its spatial partial pooling which mitigated extreme RR estimates in data-scarce areas by borrowing information from neighbouring

LHDs[14,22]. This approach reduced spurious or inflated risk estimates in low-case districts like the Far West, enhancing geographic coherence and stabilising regional risk patterns. By integrating spatial smoothing, our framework enhances the reliability of climate-influenza associations, emphasising the value of spatial epidemiological modelling in disease surveillance. Refer to supplementary section C (Fig. 11 - 19) to see how cumulative effects evolve over time in each LHD.

#### 4.2. Multi-Exposure Climate Factors and Regional Variability

Beyond temperature, midrange humidity (50–80%) emerged as a significant contributor influencing influenza risk, reinforcing evidence that moderate humidity enhances viral stability [4,5]. Although very high humidity (> 80%) was associated with sporadic spikes in non-pooled models, these were moderated by spatial smoothing, preventing inflated estimates in areas with limited data. Rainfall showed weaker and more localised associations, supporting previous findings that precipitation is secondary to temperature and humidity in short-lag influenza transmission[6].

Coastal LHDs, like Central Coast and Illawarra Shoalhaven, consistently exhibited higher probabilities of exceeding RR thresholds at moderately cool temperatures, likely due to their milder baseline climate, where even slight temperature drops have a more significant effect. In contrast, inland districts saw sharper increases in response to extreme cold or dryness, although partial pooling effectively smoothed statistical outliers. These findings underscore the importance of considering geographic variations when modelling short-term climate drivers of influenza.

#### 4.3. Strengths and limitations

Our integrated framework, combining a case-crossover design, cross-basis expansions, and hierarchical priors offers several advantages[25]. Firstly, the use of DLNM captures threshold and plateau behaviours often overlooked by linear models, while partial pooling stabilises estimates in data-sparse LHDs. Secondly, by quantifying exceedance probabilities for specific climate scenarios, this approach serves as a practical early-warning tool for outbreak mitigation.[26]

Nonetheless, we acknowledge several limitations. Aggregating climate data on a monthly basis may mask short-lived intraday fluctuations that impact viral viability [26, 27]. The reliance on case notification data introduces potential biases due to regional discrepancies in testing and reporting, likely underestimating true influenza incidence. Additionally, our focus on relative humidity rather than absolute humidity may restrict mechanistic insights into virus transmission [4]. While partial pooling addresses spatial heterogeneity, more advanced techniques such as non-stationary Gaussian processes could refine local climate-disease relationships, particularly in large or topographically diverse LHDs [28,29]. Future research should incorporate absolute humidity and socio-behavioural factors (e.g., mobility and vaccination rates) to disentangle climate related effects from other epidemiological drivers [30]. As global climate variability intensifies, such refined analytic tools will be indispensable for detecting and mitigating abrupt disease surges, thereby informing more targeted and proactive public health interventions.

## 5. Conclusion

Our analysis highlights the role of short-term climate fluctuations, particularly near-moderate temperatures, in shaping influenza dynamics in NSW. Case-crossover DLNMs with spatial partial pooling provided stable inference and spatially coherent risk maps, identifying temperature as the primary climatic driver, with humidity and rainfall showing variable but less consistent associations. By applying a spatial Bayesian DLNM, public

health officials can anticipate climate-driven influenza spikes, improving preventive measures and resource allocation. Future research should explore longer lags and additional covariates, such as mobility and vaccination, to enhance climate-influenza modelling as weather extremes intensify.

360  
361  
362  
363

## Supplementary Information

364

Supplementary Material is included in separate file. This includes additional figures and maps that support the findings of this article.

365  
366

## CRediT authorship contribution statement

367

Mohammad Afzal Khan: Conceptualisation, Data curation, Formal analysis, Interpretation of results, Initial draft of the manuscript Oyelola Adegbeye: Conceptualisation, Data curation, Interpretation of results, Contributed to drafting the manuscript, Supervision Shiyang Lyu: Contributed to drafting the manuscript Kiki Maulana Adhinugraha: Contributed to drafting the manuscript Theophilus I. Emeto: contributed to drafting the manuscript, Interpretation of results, Supervision David Taniar: Contributed to drafting the manuscript and supervision. All authors reviewed the results and approved the final version of the manuscript.

368  
369  
370  
371  
372  
373  
374  
375

## Declaration of competing interest

376

The authors declared no potential conflicts of interest with respect to the research, authorship, and/or publication of this article.

377  
378

## Data and Source Code availability

379

The data used in this study was obtained from the NSW Health Notifiable Conditions Information Management System (NCIMS). Data and source code may be available from the authors upon request. The NCIMS login portal is accessible at: <https://ncims.health.nsw.gov.au>.

380  
381  
382  
383

## Ethics

384

No specific ethics approval is required for this study. De-identified influenza data were obtained from New South Wales notifiable disease surveillance system publicly available, whilst the climate data were obtained from the Australian Bureau of Meteorology.

385  
386  
387  
388

## Funding

388

None

389

## References

1. Muscatello, D.J.; Bein, K.J.; Dinh, M.M. Influenza-associated delays in patient throughput and premature patient departure in emergency departments in New South Wales, Australia: A time series analysis. *Emergency Medicine Australasia* **2018**, *30*, 77–80. <https://doi.org/10.1111/1742-6723.12808>.  
391  
392  
393  
394  
395
2. New South Wales Ministry of Health. Influenza fact sheet – Fact sheets, 2018. Assessed: 12/08/2024.  
396  
397
3. Lowen, A.C.; Steel, J. Roles of humidity and temperature in shaping influenza seasonality. *Journal of Virology* **2014**, *88*, 7692–7695. Epub 2014 Apr 30, <https://doi.org/10.1128/JVI.03544-13>.  
398  
399
4. Shaman, J.; Kohn, M. Absolute humidity modulates influenza survival, transmission, and seasonality. *Proceedings of the National Academy of Sciences of the United States of America* **2009**, *106*, 3243–3248. <https://doi.org/10.1073/pnas.0806852106>.  
400  
401  
402
5. Tamerius, J.D.; Shaman, J.; Alonso, W.J.; Bloom-Feshbach, K.; Uejio, C.K.; Comrie, A.; Viboud, C. Environmental predictors of seasonal influenza epidemics across temperate and tropical climates. *PLoS Pathogens* **2013**, *9*, e1003194. <https://doi.org/10.1371/journal.ppat.1003194>.  
403  
404  
405
6. Yan, Z.; Liu, W.; Long, Y.; Ming, B.; Yang, Z.; Qin, P.; Ou, C.; Li, L. Effects of meteorological factors on influenza transmissibility by virus type/subtype. *BMC Public Health* **2024**, *24*, 494. <https://doi.org/10.1186/s12889-024-17961-9>.  
406  
407  
408
7. Yin, Y.; Lai, M.; Zhou, S.; Chen, Z.; Jiang, X.; Wang, L.; Li, Z.; Peng, Z. Effects and interaction of temperature and relative humidity on the trend of influenza prevalence: A multi-central study based on 30 provinces in mainland China from 2013 to 2018. *Infectious Disease Modelling*, 2023. <https://doi.org/10.1016/j.idm.2023.07.005>.  
409  
410  
411  
412
8. Wang, X.; Kim, K.W.; Walker, G.; Stelzer-Braids, S.; Scotch, M.; Rawlinson, W.D. Genome characterization of influenza A and B viruses in New South Wales, Australia, in 2019: A retrospective study using high-throughput whole genome sequencing. *Influenza and Other Respiratory Viruses* **2024**, *18*, e13252. Epub 2024 Jan 5, <https://doi.org/10.1111/irv.13252>.  
413  
414  
415  
416
9. Immunisation Coalition. Influenza statistics, 2024. Retrieved September 9, 2024.  
417
10. Taouk, M. NSW's flu season drags on longer than previous years as jabs become 'less of a priority' 2023.  
418  
419
11. Bhaskaran, K.; Gasparrini, A.; Hajat, S.; Smeeth, L.; Armstrong, B. Time series regression studies in environmental epidemiology. *International Journal of Epidemiology* **2013**, *42*, 1187–1195. <https://doi.org/10.1093/ije/dyt092>.  
420  
421  
422
12. Basu, R.; Sarover, V.; Malig, B.J. Association Between High Ambient Temperature and Risk of Stillbirth in California. *American Journal of Epidemiology* **2016**, *183*, 894–901. <https://doi.org/10.1093/aje/kwv295>.  
423  
424  
425
13. Gasparrini, A.; Armstrong, B.; Kenward, M.G. Distributed lag non-linear models. *Statistics in Medicine* **2010**, *29*, 2224–2234. <https://doi.org/10.1002/sim.3940>.  
426  
427
14. Waller, L.A.; Gotway, C.A. *Applied Spatial Statistics for Public Health Data*; Wiley Series in Probability and Statistics, John Wiley & Sons, Inc.: Hoboken, NJ, 2004. <https://doi.org/10.1002/0471662682>.  
428  
429  
430
15. Quijal-Zamorano, M.; Martinez-Beneito, M.A.; Ballester, J.; Marí-DellOlmo, M. Spatial Bayesian distributed lag non-linear models (SB-DLNM) for small-area exposure-lag-response epidemiological modelling. *International Journal of Epidemiology* **2024**, *53*. <https://doi.org/10.1093/ije/dya061>.  
431  
432  
433  
434
16. Charland, K.M.; Buckeridge, D.L.; Sturtevant, J.L.; Melton, F.; Reis, B.Y.; Mandl, K.D.; Brownstein, J.S. Effect of environmental factors on the spatio-temporal patterns of influenza spread. *Epidemiology and Infection* **2009**, *137*, 1377–1387. <https://doi.org/10.1017/S0950268809002283>.  
435  
436  
437
17. Mahmud, A.S.; Martinez, P.P.; Baker, R.E. The impact of current and future climates on spatiotemporal dynamics of influenza in a tropical setting. *PNAS Nexus* **2023**. <https://doi.org/10.1093/pnasnexus/pgad307>.  
438  
439  
440
18. Chadsuthi, S.; Iamsirithaworn, S.; Triampo, W.; Modchang, C. Modeling Seasonal Influenza Transmission and Its Association with Climate Factors in Thailand Using Time-Series and  
441  
442

- ARIMAX Analyses. *Computational and Mathematical Methods in Medicine* **2015**. <https://doi.org/10.1155/2015/436495>. 443  
444
19. New South Wales Ministry of Health. Disease notification. NSW Health Notifiable Conditions Information Management System (NCIMS), 2024. Available from: <https://www.health.nsw.gov.au/Infectious/Pages/notification.aspx> Assessed: 12/08/2024. 445  
446  
447
20. Maclure, M. The case-crossover design: a method for studying transient effects on the risk of acute events. *American Journal of Epidemiology* **1991**, *133*, 144–153. <https://doi.org/10.1093/oxfordjournals.aje.a115853>. 448  
449  
450
21. Madaniyazi, L.; Tobías, A.; Vicedo-Cabrera, A.M.; et al. Should we adjust for season in time-series studies of the short-term association between temperature and mortality? *Epidemiology* **2023**, *34*, 313–318. <https://doi.org/10.1097/EDE.0000000000001592>. 451  
452  
453
22. Gelman, A.; Carlin, J.B.; Stern, H.S.; Dunson, D.B.; Vehtari, A.; Rubin, D.B. *Bayesian Data Analysis*, 3rd ed.; Chapman and Hall/CRC Texts in Statistical Science, CRC Press: Boca Raton, FL, 2013. 454  
455  
456
23. Liang, M.; Li, Z.; Zhang, L.; Wang, M. A SpatialTemporal Bayesian Model for a Case-Crossover Design with Application to Extreme Heat and Claims Data. *Stats* **2024**, *7*, 1379–1391. <https://doi.org/10.3390/stats7040080>. 457  
458  
459
24. Soebiyanto, R.P.; Adimi, F.; Kiang, R.K. Modeling and predicting seasonal influenza transmission in warm regions using climatological parameters. *PLoS ONE* **2010**, *5*, e9450. <https://doi.org/10.1371/journal.pone.0009450>. 460  
461  
462
25. Yin, F.; Zhang, T.; Liu, L.; et al.. The Association between Ambient Temperature and Childhood Hand, Foot and Mouth Disease in Chengdu, China: A Distributed Lag Non-linear Analysis. *Scientific Reports* **2016**, *6*, 27305. PMCID: PMC4907949, <https://doi.org/10.1038/srep27305>. 463  
464  
465
26. Ballester, J.; van Daalen, K.R.; Chen, Z.; et al.. The effect of temporal data aggregation to assess the impact of changing temperatures in Europe: an epidemiological modelling study. *The Lancet Regional Health – Europe* **2024**, *36*, 100779. <https://doi.org/10.1016/j.lanepe.2023.100779>. 466  
467  
468
27. Hilbe, J.M. *Modeling Count Data*; Cambridge University Press: Cambridge, 2014. <https://doi.org/10.1017/CBO9781139236065>. 469  
470  
471
28. Abdul-Fattah, E.; Krainski, E.T.; van Niekerk, J.; Rue, H. Non-stationary Bayesian spatial model for disease mapping based on sub-regions. *Statistical Methods in Medical Research* **2024**, *33*, 1093–1111. <https://doi.org/10.1177/09622802241244613>. 472  
473
29. Ejigu, B.A.; Wencheko, E.; Moraga, P.; Giorgi, E. Geostatistical methods for modelling non-stationary patterns in disease risk. *Spatial Statistics* **2020**, *35*, 100397. <https://doi.org/10.1016/j.spasta.2019.100397>. 474  
475  
476
30. Marsh, C.K.; Sheppeard, V.; Tobin, S.; Gilmour, R.; Andrews, R.M. Drivers of the summer influenza epidemic in New South Wales, 2018–19, 2022. Epub 2021 Sep 21, <https://doi.org/10.5694/mja2.51266>. 477  
478  
479